RSC Advances

Cite this: *RSC Advances*, 2012, **2**, 5927–5929

www.rsc.org/advances

COMMUNICATION

Core-shell structured sulfur-polypyrrole composite cathodes for lithium-sulfur batteries†

Yongzhu Fu and Arumugam Manthiram*

Received 5th March 2012, Accepted 2nd May 2012
DOI: 10.1039/c2ra20393f

A sulfur-polypyrrole composite cathode with a core-shell structure consisting of spherical sulfur particles coated with polypyrrole has been developed. The conductive polypyrrole coating on the sulfur facilitates fast electron transport enabling the material with superior electrochemical stability, rate capability, and cyclability in lithium-sulfur batteries.

Electrical energy storage is critical for the efficient utilization of renewable energies, *e.g.*, solar and wind. Vehicle electrification also requires advanced electrical energy storage technologies that can offer high energy and high power densities. Lithium-ion (Li-ion) batteries offer the highest energy densities among the known battery systems and are believed to be the most viable near-term option for these applications.[1,2] Despite their success in the portable electronics market, there are a number of issues such as cost, safety, and energy density that impede the practical application of large-format Li-ion cells. Development of alternative cathodes with higher capacity and better safety than conventional intercalation cathodes (*e.g.*, $LiCoO_2$, Li_2MnO_4, $LiFePO_4$) is needed for the Li-ion technology to be successful for large-scale applications.

Sulfur, one of the most abundant elements on earth, offers a high theoretical capacity of 1675 mA h g^{-1}, making it a potential high capacity cathode material for Li-ion batteries.[3] More importantly, its low operating voltage of ~2.1 V could offer safety advantages over the high-voltage intercalation cathodes (>3.3 V). However, sulfur is an insulator with a very low electrical conductivity of 10^{-30} S cm^{-1}, making it difficult to achieve high active material utilization within the electrodes. Lithium polysulfides (Li_2S_x, x = 8, 6, 5, and 4) produced during charge-discharge cycles are soluble in the liquid electrolyte, resulting in a significant morphology and compositional changes within the electrodes along with the shuttling mechanism of transporting polysulfides between the cathode and anode.[4,5] To overcome these problems, two effective strategies have been developed: one strategy is to prepare composite electrodes with other conductive materials, such as carbon nanotubes,[6,7] graphene,[8,9] porous carbon,[10–14] and conductive polymers.[15,16] Another strategy is to prepare core-shell structures in which sulfur is the core and conductive materials are the shell, offering effective electrochemical contact, shorter path length for ion and electron transport, more freedom for compositional change, and better reaction kinetics at the electrode surface.[17,18] For example, Jayaprakash *et al.*[17] developed a template approach for synthesizing mesoporous hollow carbon capsules that can encapsulate elemental sulfur in its porous shell. The material exhibited a reversible capacity of 974 mA h g^{-1} at a rate of 0.5 C with 91% capacity retention after 100 cycles and a maximum discharge rate of 3 C.[17] Wu *et al.*[18] developed core-shell structured sulfur-polythiophene composites showing improved electrochemical performance and rate capability at <1 C. However, this approach utilized commercial sulfur with large particle size (>20 μm) and irregular shape, making the interior bulk sulfur inaccessible to electrons and the electrolyte.

Here, we present a facile and scalable route to fabricate core-shell structured sulfur-polypyrrole (S-PPy) composites consisting of spherical sulfur particles with uniform particle size coated with conductive polypyrrole. The sulfur in the core contains pores that allow electrolyte to access the bulk sulfur. The conductive polypyrrole skin on the sulfur particles facilitates efficient charge transport, supporting high rate capability, suppressing the loss of active materials, and maintaining excellent cyclability.

First, elemental sulfur was synthesized by reducing sodium thiosulfate with *p*-toluenesulfonic acid (*p*TSA), as shown in Fig. 1a. The sulfonic acid on the *p*TSA provides protons while forming micelles for sulfur to nucleate, as an anionic surfactant. The formed sulfur particles have uniform spherical shape with a diameter of 5–10 microns as seen in Fig. 1b. The magnified SEM image in Fig. 1b reveals that small pores are present on the surface of sulfur particles, which could be beneficial for the electrolyte to access the inner bulk sulfur. The synthesized sulfur was then added to an aqueous solution containing decyltrimethylammonium bromide (DeTAB), which is known to be a cationic surfactant for the synthesis of nanosized spherical polypyrrole with a particle size of ~100 nm.[19] The synthesized polypyrrole nanoparticles are believed to nucleate onto sulfur particles with the aid of DeTAB, as shown in Fig. 1a. After the removal of the surfactant, sulfur coated with a layer of polypyrrole was obtained as clearly revealed by the SEM images of Fig. 1c, 1d, and Fig. S1.

The sulfur and S-PPy composite were characterized by X-ray diffraction (XRD), as shown in Fig. 2a. The XRD pattern of sulfur matches with that in the literature for *Fddd* orthorhombic sulfur.[20] The S-PPy composite shows a similar pattern although slightly less defined due to the polypyrrole coating. To determine the sulfur

Electrochemical Energy Laboratory & Materials Science and Engineering Program, The University of Texas at Austin, Austin, TX 78712, United States. E-mail: rmanth@mail.utexas.edu

† Electronic supplementary information (ESI) available. See DOI: 10.1039/c2ra20393f

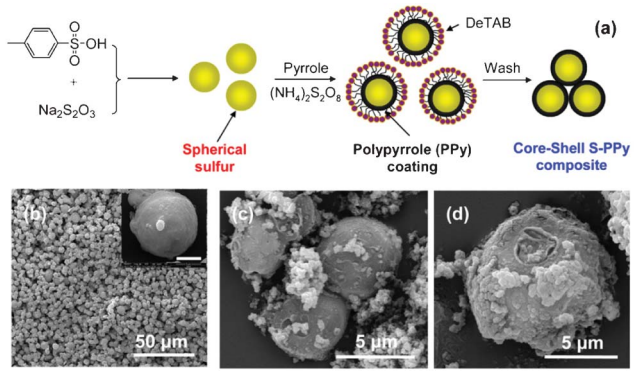

Fig. 1 (a) Schematic illustration of the synthesis process of core-shell structured sulfur-polypyrrole (S-PPy) composites with the use of the cationic surfactant decyltrimethylammonium bromide (DeTAB), (b) scanning electron microscopy (SEM) image of the spherical sulfur particles with the inset showing a magnified SEM image of a single sulfur particle with a scale bar of 5 μm, (c) SEM image of a few S-PPy composite particles, and (d) SEM image of a single S-PPy particle.

content in the S-PPy composites, pristine PPy and two composite samples with different pre-calculated sulfur (70 and 80 wt%) were prepared and analyzed by thermogravimetric analysis (TGA) as shown in Fig. 2b. Sulfur exhibits a single weight loss profile, which starts at its melting temperature (*i.e.*, 115 °C). Pristine PPy is observed to exhibit two distinct weight loss profiles. The first one starts at 30 °C, which is due to the elimination of residual water in the sample, and the second major weight loss starts at 220 °C, which is due to the decomposition of PPy.[21] The S-PPy composite exhibits a combination of the weight loss processes of pristine sulfur and PPy, showing three weight loss profiles. The second weight loss starts at temperatures below 115 °C, which could be due to the bonding of sulfur to polypyrrole. The actual sulfur contents within these two composites are, respectively, 65.8 and 77.0 wt%. Hereafter, these two S-PPy composites are denoted as, respectively, S-PPy-65 and S-PPy-77.

Fig. 2c compares the X-ray photoelectron spectra (XPS) of the S-PPy composite and Fig. 2d compares the S 2p peaks of the S-PPy composite before and after the depth profiling analysis (sputtering). In Fig. 2c, the N 1s (398.8 eV) and C 1s (284.8 eV) peaks can be attributed to the nitrogen and carbon on the polypyrrole.[22] The strong O 1s peak in Fig. 2c and the broad peak at 166–170 eV in Fig. 2d before sputtering are assigned to the oxygen of the sulfonate group on *p*TSA,[23] which is the residual reactant from the sulfur formation reaction and present on the surface of sulfur particles. It is believed that the polypyrrole could be doped with *p*TSA in the coating layer, which has an electrical conductivity of $\sim 6 \times 10^{-2}$ S cm^{-1}.[24] The sputtering penetrates a depth of $\sim$100 nm, which is equivalent to the thickness of polypyrrole nanospheres formed under the synthesis conditions. After sputtering, the intensities of both S 1s and S 2p peaks increase in Fig. 2d as sulfur becomes more exposed to the surface. In addition, the O 1s peak associated with the sulfonate group on *p*TSA has almost vanished in Fig. 2d, revealing that the *p*TSA is present only within the polypyrrole coating. In Fig. 2d, the dual peaks at 164.7 and 163.5 eV with an intensity ratio of $\sim 1:2$ are due to spin orbit coupling and are characteristic of S $2p_{1/2}$ and $2p_{3/2}$.[25] These results confirm that the *p*TSA is present with polypyrrole on the shell while the elemental sulfur is mostly present in the core, implying that the synthesized S-PPy composite has a core-shell structure.

To study the electrochemical properties of the S-PPy-65 composite, CR2032 coin cells with metallic lithium anode were assembled and evaluated. Fig. 3a shows the first three cyclic voltammograms (CV) of the cell. The two separated reduction peaks at 2.4 and 2.1 V correspond to the conversion of, respectively, high-order lithium polysulfides (*e.g.*, Li_2S_8) to low-order lithium polysulfides (Li_2S_x, $8 > x \geqslant 4$) and lithium polysulfides to solid-state Li_2S_2/Li_2S. However, only one oxidation peak is seen, implying the

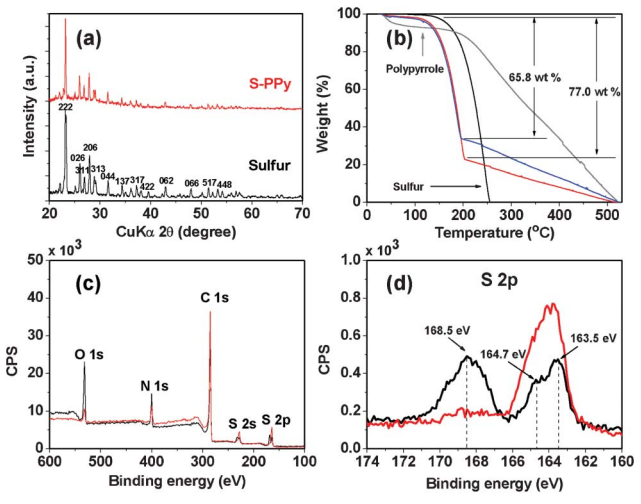

Fig. 2 (a) XRD patterns of sulfur (black) and the S-PPy composite (red), (b) thermogravimetric analysis (TGA) of sulfur (black), pristine PPy (grey), and S-PPy composites (red and blue), showing up to 77 wt% of sulfur contained within the composites, (c) XPS of S-PPy composite before (black) and after (red) sputtering, and (d) S 2p characteristic peaks in the XPS of S-PPy composite before (black) and after (red) sputtering.

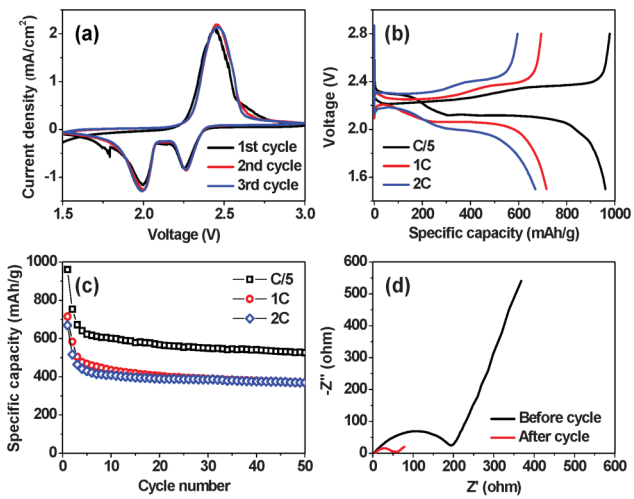

Fig. 3 (a) First three cyclic voltammograms (CV) of the S-PPy-65 composite at a sweep rate of 0.2 mV s^{-1}, (b) first discharge and charge voltage *vs.* specific capacity profiles at 2.8–1.5 V at various C rates (C/5, 1C, and 2C) (the capacity values are in terms of the percentage of the sulfur active mass), (c) cyclability of the S-PPy-65 composite at various C rates (C/5, 1C, and 2C), and (d) impedance analysis of the cells containing the S-PPy composite electrode before (black) and after (red) 50 cycles.

transformation of all the polysulfides into the intermediate, which is believed to be S_8^{2-} with the most facile oxidation kinetics.[26] More importantly, these peaks remain rather constant upon cycling, indicating the excellent electrochemical stability of the S-PPy composite as the polypyrrole shell protects the core sulfur and thereby suppresses the loss of active materials and reduces the shuttling phenomenon during the charge-discharge cycles.[4] Similarly, the CV of the S-PPy-77 composite in Fig. S3 also shows very stable peaks. In contrast, the CV of the pristine sulfur electrode shows decreasing and shifting peaks as shown in Fig. S2. Thus, the polypyrrole coating acts as a protection barrier, suppressing the dissolution of lithium polysulfides into the liquid electrolyte and making the S-PPy composites electrochemically stable.

Fig. 3b presents the initial discharge and charge voltage profiles *vs.* specific capacities of sulfur at rates of C/5, 1C, and 2C. The two discharge voltage plateaus resemble the peaks in the CVs. The first discharge capacity at C/5 is >900 mA h g^{-1} while the capacities at high rates are >600 mA h g^{-1}. The complete first charge profiles also prove that the polypyrrole coating suppresses the shuttling phenomenon.[4] Part of the total capacity could be due to polypyrrole in the potential range studied, but it would be minimal.[27] Fig. 3c further compares the cycle life of the S-PPy-65 composite. The material exhibits a reduction in discharge capacity from 961 to 672 mA h g^{-1} at C/5 during the first three cycles; similarly, it exhibits a reduction of ~200 mA h g^{-1} at 1C and 2C rates during the first three cycles. Afterwards, the cathode maintains a relatively constant capacity of ~600 mA h g^{-1} at C/5. Obviously, the cathode maintains a very stable capacity of >400 mA h g^{-1} at higher rates of 1C and 2C, which could not be obtained with conventional pristine sulfur electrodes. The S-PPy-77 composite also shows similar cyclability behavior as the S-PPy-65 composite in Fig. S4 but with lower capacities due to the inefficient coating of polypyrrole on the sulfur particles. As a result, at the beginning of the cycling, some lithium polysulfides formed could dissolve into the liquid electrolyte, resulting in a loss of capacity. Afterwards, the polypyrrole coating could become a stable interface between the liquid electrolyte and lithium polysulfides, allowing fast ion and charge transfer with minimum loss of active materials. This process is evidenced by the electrochemical impedance analysis shown in Fig. 3d for the S-PPy-65 composite and in Fig. S5 for the S-PPy-77 composite. The semicircles are ascribed to charge transfer resistance within the electrodes.[28] It can be clearly seen that the charge transfer resistance decreases significantly after 50 cycles from 200 to 60 ohms, indicating the improved conducting property of the electrodes due to the polypyrrole coating. The superior electrochemical performance of the S-PPy composites can be attributed to the core-shell structure with the conductive polypyrrole coating providing a fast and efficient transport of lithium ions and charge transfer within the electrodes.

In summary, we have developed a facile solution-phase route for the fabrication of sulfur-polypyrrole composites with a core-shell structure. The spherical sulfur could readily be coated with a conductive polypyrrole layer with a thickness of ~100 nm. The S-PPy composites exhibit excellent rate capability with good cyclability, making them attractive cathodes for lithium-ion batteries.

This work was supported by Seven One Limited. The authors thank Thomas Cochell for his assistance with the XPS analysis.

References

1 B. Scrosati and J. Garche, *J. Power Sources*, 2010, **195**, 2419.
2 Z. Yang, J. Zhang, M. C. W. Kintner-Meyer, X. Lu, D. Choi, J. P. Lemmon and J. Liu, *Chem. Rev.*, 2011, **111**, 3577.
3 B. L. Ellis, K. T. Lee and L. F. Nazar, *Chem. Mater.*, 2010, **22**, 691.
4 Y. V. Mikhaylik and J. R. Akridge, *J. Electrochem. Soc.*, 2004, **151**, A1969.
5 J. R. Akridge, Y. V. Mikhaylik and N. White, *Solid State Ionics*, 2004, **175**, 243.
6 L. Yuan, H. Yuan, X. Qiu, L. Chen and W. Zhu, *J. Power Sources*, 2009, **189**, 1141.
7 J. Guo, Y. Xu and C. Wang, *Nano Lett.*, 2011, **11**(10), 4288.
8 H. Wang, Y. Yang, Y. Liang, J. T. Robinson, Y. Li, A. Jackson, Y. Cui and H. Dai, *Nano Lett.*, 2011, **11**(7), 2644.
9 Y. Cao, X. Li, I. A. Aksay, J. Lemmon, Z. Nie, Z. Yang and J. Liu, *Phys. Chem. Chem. Phys.*, 2011, **13**, 7660.
10 C. Liang, N. J. Dudney and J. Y. Howe, *Chem. Mater.*, 2009, **21**, 4724.
11 X. Ji, K. T. Lee and L. F. Nazar, *Nat. Mater.*, 2009, **8**, 500.
12 S. Wei, H. Zhang, Y. Huang, W. Wang, Y. Xia and Z. Yu, *Energy Environ. Sci.*, 2011, **4**, 736.
13 G. He, X. Ji and L. F. Nazar, *Energy Environ. Sci.*, 2011, **4**, 2878.
14 C. Lai, X. P. Gao, B. Zhang, T. Y. Yan and Z. Zhou, *J. Phys. Chem. C*, 2009, **113**, 4712.
15 X. Liang, Y. Liu, Z. Wen, L. Huang, X. Wang and H. Zhang, *J. Power Sources*, 2011, **196**, 6951.
16 J. Wang, J. Chen, K. Konstantinov, L. Zhao, S. H. Ng, G. X. Wang, Z. P. Guo and H. K. Liu, *Electrochim. Acta*, 2006, **51**, 4634.
17 N. Jayaprakash, J. Shen, S. S. Moganty, A. Corona and L. A. Archer, *Angew. Chem., Int. Ed.*, 2011, **50**, 5904.
18 F. Wu, J. Chen, R. Chen, S. Wu, L. Li, S. Chen and T. Zhao, *J. Phys. Chem. C*, 2011, **115**, 6057.
19 J. Jang, J. H. Oh and G. D. Stucky, *Angew. Chem., Int. Ed.*, 2002, **41**, 4016.
20 S. J. Rettig and J. Trotter, *Acta Crystallogr., Sect. C: Cryst. Struct. Commun.*, 1987, **43**, 2260.
21 P. Mavinakuli, S. Wei, Q. Wang, A. B. Karki, S. Dhage, Z. Wang, D. P. Young and Z. Guo, *J. Phys. Chem. C*, 2010, **114**, 3874.
22 C. Malitesta, I. Losito, L. Sabbatini and P. G. Zambonin, *J. Electron Spectrosc. Relat. Phenom.*, 1995, **76**, 629.
23 O. Bubnova, Z. U. Khan, A. Malti, S. Braun, M. Fahlman, M. Berggren and X. Crispin, *Nat. Mater.*, 2011, **10**, 429.
24 S. Goel, N. A. Mazumdar and A. Gupta, *Polym. Adv. Technol.*, 2010, **21**, 205.
25 Y. Yang, G. Yu, J. J. Cha, H. Wu, M. Vosgueritchian, Y. Yao, Z. Bao and Y. Cui, *ACS Nano*, 2011, **5**, 9187.
26 X. Ji and L. F. Nazar, *J. Mater. Chem.*, 2010, **20**, 9821.
27 B. Guo, Q. Kong, Y. Zhu, Y. Mao, Z. Wang, M. Wan and L. Chen, *Chem.–Eur. J.*, 2011, **17**, 14878.
28 V. S. Kolosnitsyn, E. V. Kuz'mina, E. V. Karaseva and S. E. Mochalov, *Russ. J. Electrochem.*, 2011, **47**, 793.